Colloidal Dispersions of Gold Rods: Synthesis and Optical Properties

Bianca M. I. van der Zande,[†,‡] Marcel R. Böhmer,*[,†]
Lambertus G. J. Fokkink,[†,§] and Christian Schönenberger[†,||]

Philips Research Laboratories, Prof. Holstlaan 4, 5656 AA Eindhoven, The Netherlands, Van't Hoff Laboratory for Physical and Colloid Chemistry, Debye Institute, Utrecht University, Padualaan 8, 3584 CH Utrecht, The Netherlands

Received January 14, 1999. In Final Form: August 23, 1999

Colloidal dispersions of rod-shaped gold particles are obtained by electrodeposition of gold in the nanopores of anodized alumina attached to a conductive support followed by dissolution of the alumina and release of the rods from the support. Coagulation is prevented by steric repulsion due to adsorption of poly(vinylpyrrolidone) on the gold surface. The synthesis method presented is suitable for the preparation of dispersions of nearly monodisperse colloidal gold rods with adjustable aspect ratio L/d in the range $1.8 < L/d < 49$. The length, L, is tuned between 39 and 729 nm, and the diameter, d, is between 12 and 22 nm. The absorbance spectra of randomly oriented colloidal gold rods display a transverse and a longitudinal resonance contribution. With increasing aspect ratio, the transverse resonance shows a small shift to shorter wavelengths, while the longitudinal resonance shifts into the near-infrared regime. The positions of the absorbance maxima agree with the predictions of the Gans theory.

Introduction

In the past decade several methods have been developed to obtain liquid dispersions of rod-shaped metal particles.[1−5] The synthesis of rod-shaped metallic colloidal particles often requires a template because thermodynamics in general favors a spherical growth mode for small particles. Available templates are rod-shaped (inverted) micelles,[1−4] the so-called soft templates, or nanoporous membranes (hard templates).[6−15] The use of soft templates directly results in a dispersion of rod-shaped particles by UV irradiation. Hard templates require subsequent steps in which the solid template has to be replaced by a liquid in order to obtain a dispersion. The advantage of hard templates is that it allows for easy adjustment of the length. Furthermore, the pore diameter can be increased by slow dissolution of the hard template, enabling the preparation of rods with different sizes but the same aspect ratio. Extensive documentation is available for the electrodeposition of many metals in hard templates[6−15] because these (partially) filled membranes show, depending on the deposited material, interesting properties such as dichroism[7,13] or strong perpendicular magnetic anisotropy.[8−10]

When rod-shaped particles are dispersed in a liquid instead of a solid, Brownian motion will occur, resulting in randomly oriented particles in the continuous phase. This allows investigation of their dynamical behavior and their optical properties in a random orientation. Furthermore, anisotropic particles dispersed in fluids are sensitive to external fields, which may lead to birefringence or optical switching.[16−18] Optical properties of metal rods can be modeled using the Gans theory,[19] which is an extension of the Mie theory[20] with a geometrical factor. This theory demonstrates that for elongated ellipsoids the direction of the plasmon oscillation depends on the orientation of the particle axis with respect to the wavevector of incident light as shown in Figure 1. This results in two absorbance maxima designated as the transverse resonance[7,21−23] and the longitudinal resonance[21−25] instead of the single absorbance maximum for

* Corresponding author.
† Philips Research Laboratories.
‡ Utrecht University.
§ Present address: Gintic Institute of Manufacturing Technology, 71 Nanyang Drive, Singapore 638075, Singapore.
|| Present address: Institute for Physics, University Basel, Klingelbergstrasse 82, CH-4056 Basel, Switzerland.

(1) Tanori, J.; Pileni, M. P. *Langmuir* **1997**, *13*, 639.
(2) Esumi, K.; Matsuhisa, K.; Torigoe, K. *Langmuir* **1995**, *11*, 3285.
(3) Yu, Y.; Chang, S.; Lee, C.; Wang, C. R. *J. Phys. Chem. B* **1997**, *101*, 6661.
(4) Chang, S. S.; Shih, C. W.; Chen, C. D.; Lai, W. C.; Wang, C. R. C. *Langmuir* **1999**, *15*, 701.
(5) Lickes, J.-P.; Dumont, F.; Buess-Herman, C. *Colloids Surf. A* **1996**, *118*, 167.
(6) Whitney, T. M.; Jiang, J. S.; Searson, P. C.; Chien, C. L. *Science* **1993**, *261*, 1316.
(7) Foss, C. A.; Hornyak, G. L.; Stockert, J. A.; Martin, C. R. *J. Phys. Chem.* **1994**, *98*, 2963.
(8) Tsuya, N.; Tokushima, T.; Shiraki, M.; Wakui, Y.; Saito, Y.; Nakamura, H.; Harada, Y. *IEEE Trans. Magn.* **1988**, *24*, 2661. Tsuya, N.; Tokushima, T.; Shiraki, M.; Wakui, Y.; Saito, Y.; Nakumara, H.; Katsumata, Y. *IEEE Trans. Magn.* **1987**, *23*, 53.
(9) Shiraki, M.; Wakui, Y.; Tokushima, T.; Tsuya, N. *IEEE Trans. Magn.* **1985**, *21*, 1465.
(10) Arai, K. I.; Kang, H. W.; Ishiyama, K. *IEEE Trans. Magn.* **1991**, *27*, 4906.
(11) Martin, C. R. *Science* **1994**, *266*, 1961.
(12) Schönenberger, C.; van der Zande, B. M. I.; Fokkink, L. G. J.; Henny, M.; Schmid, C.; Krüger, M.; Bachtold, A.; Huber, R.; Birk, H.; Staufer, U. *J. Phys. Chem. B* **1997**, *101*, 5497.
(13) Foss, C. A.; Tierney, M. J.; Martin, C. R. *J. Phys. Chem.* **1992**, *96*, 9001.
(14) Al-Rawadesh, N. A. F.; Sandrock, M. L.; Seugling, C. J.; Foss, C. A., Jr. *J. Phys. Chem. B* **1998**, *102*, 361.
(15) Hulteen, J. C.; Martin, C. R. *J. Mater. Chem.* **1997**, *7*, 1075.
(16) Saxe, R. L.; Thompson, R. I. *Res. Front.* **1996**, Apr/May (http://www.refr-spd.com/article.html).
(17) Saito, Y.; Hirata, M.; Tada, H.; Hyodo, M. *Appl. Phys. Lett.* **1993**, *63*, 1319.
(18) van de Zande, B. M. I.; Koper, G. J. M.; Lekkerkerker, H. N. W. *J. Phys. Chem. B* **1999**, *103*, 5754.
(19) Gans, R. *Ann. Phys.* **1912**, *37*, 881; **1915**, *47*, 270.
(20) Mie, G. *Ann. Phys.* **1908**, *25*, 377.
(21) Lebedeva, V. N.; Distler, G. I. *Opt. Spectrosc.* **1967**, *23*, 527.
(22) Blatchford, C. G.; Campbell, J. R.; Creighton, J. A. *Surf. Sci.* **1982**, *120*, 435.
(23) van der Zande, B. M. I.; Böhmer, M. R.; Fokkink, L. G. J.; Schönenberger, C. *J. Phys. Chem. B* **1997**, *101*, 852.
(24) Skillman, D. C.; Berry, C. R. *J. Chem. Phys.* **1968**, *48*, 3297.
(25) Creighton, J. A.; Eadon, D. G. *J. Chem. Soc., Faraday Trans.* **1991**, *87*, 3881.

10.1021/la9900425 CCC: $19.00
Published on Web 11/16/1999

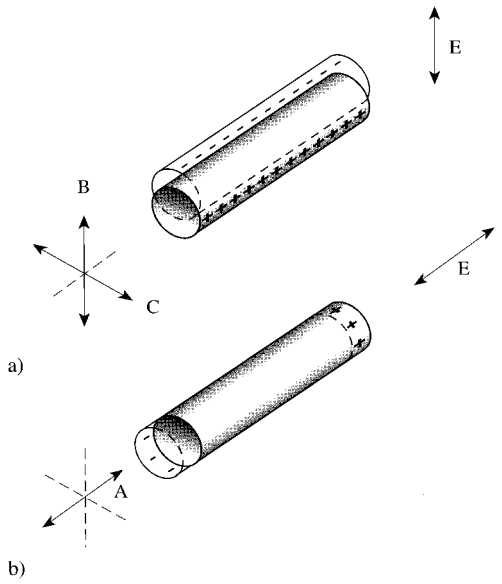

Figure 1. Schematic representation of the plasmon resonance in anisotropic particles. *E* is the oscillating electric field of the incident light. For a rodlike particle, two oscillation modes are possible: (a) the transverse oscillation (along the *B* or *C* axis) and (b) the longitudinal oscillation (along the *A* axis). The plasmon oscillation induces a dipole by local, temporary charge separation.

the spherical gold dispersion. The Gans theory predicts that the longitudinal resonance shifts to longer wavelengths with increasing aspect ratio (length *L* over diameter *d*), whereas the transverse resonance shifts to slightly shorter wavelengths.

Experimental evidence supporting the Gans theory was obtained by Skillman et al.,[24] who studied the optical properties of silver ellipsoids embedded in gelatin. Indeed, a shift of the longitudinal resonance is found for longer wavelengths with increasing aspect ratio of the particles. Moreover, the wavelength at which the absorbance maximum occurs agrees with the wavelength predicted by Gans. Agreement with the Gans theory is also obtained for gold particles dispersed in a poly(vinyl alcohol) film.[21,26,27] Foss et al.[7] studied the transverse resonance of colloidal gold rods embedded in a porous alumina membrane. The transverse resonance band shifted to slightly shorter wavelengths with increasing aspect ratio.

The above-mentioned studies were all performed on particles which are embedded in a solid medium. The aim of this paper is to prepare *aqueous dispersions* of colloidal gold rods and study their optical properties. Therefore, in this study, we focus on the release of the rods from the membrane to an aqueous medium and on the stabilization of the dispersed particles before the optical properties are studied. A porous alumina template prepared by anodization of aluminum[7−10] was used as the template for the electrodeposition of gold. Under appropriate circumstances, this method enables the synthesis of dispersions of nearly monodisperse gold particles of adjustable aspect ratio.[7,13]

In this paper we first describe the preparation of the gold rod dispersion, starting from the anodization of an aluminum substrate, the electrochemical deposition of gold followed by dissolution of Al_2O_3, and release of the rods in the presence of PVP in an aqueous continuous phase.

Table 1. Vacuum Vapor Deposition Circumstances and the Layer Thicknesses of the Ti Adherence Layer, Pt Electrode, and Al Layer

	layer thickness (nm)	deposition rate (nm/s)	pressure (10^{-10} bar)
Ti	10	0.1	2−3
Pt	75	0.2	2−3
Al	1000	2	1.5−7

Subsequently, the model used to study the optical properties is outlined. The rods are characterized by analysis of transmission electron microscope (TEM) pictures, and the spectra are given and discussed within the framework of the optical theory.

Experimental Section

Materials. Copper(II) sulfate ($Cu_2SO_4 \cdot 5H_2O$), citric acid ($C_6H_8O_7$), potassium hydroxide (KOH), and sodium hydroxide (NaOH) were purchased from Merck. Potassium gold(I) cyanide ($KAuCN_2$) was obtained from H. Drijfhout & Zoon's, Edel-metaal bedrijven B.V., The Netherlands. Sulfuric acid (95−97% H_2SO_4), phosphoric acid (85% H_3PO_4), and hydrogen peroxide (containing 30% H_2O_2) were all obtained from Merck. Poly(vinylpyrrolidone) (PVP; K30-PVP, $M_w = 40\,000$) was purchased from Fluka. All chemicals were used without further purification. In all preparation and rinsing stages, demineralized water was used.

Preparation of the Porous Alumina Template. *Substrate.* The support used in the synthesis consisted of a silicon wafer which was segmented into pieces of size 14 × 14 mm^2. Subsequently, 10 nm titanium, 75 nm platinum, and 1 μm aluminum were vacuum evaporated on the silicon wafer. Table 1 summarizes the conditions of the vacuum evaporation. Titanium ensures the adherence of the platinum working electrode on the silicon substrate. Prior to the vacuum evaporation of aluminum, the substrate was cooled until the substrate temperature reached room temperature again. This turned out to be crucial to obtain smooth aluminum layers and, consequently, well-defined pores.

Anodization. Porous alumina was obtained by anodization of aluminum at a constant voltage of 15 V in 15 v/v % H_2SO_4 at room temperature.[10,28,29] The setup of the anodization process is given in Figure 2. The substrate was mounted on the bottom of the Teflon cell (1), with the aluminum facing up serving as the working electrode (6). Only the center part of the aluminum was exposed to the electrolyte constrained by an O-ring seal (5) with a diameter of 9 mm. A voltage of 15 V was applied with a power supply (EK 030-10, Delta Elektronika) between the working electrode and the platinum counter electrode (3) with a surface area of about 6 cm^2. Stirring, required to anodize the aluminum homogeneously, was performed with a rotating disk (2) with a diameter of 1 cm at a rotation rate of 3000 rpm. The stirrer was placed approximately 1 cm above the working electrode. The anodization process was monitored by measuring the current as a function of time using a Philips PM 2534 system multimeter and a Philips PM 8222 dual pen recorder. Figure 3 shows a typical current−time curve. At a current density of 35 mA·cm^{-2} at 293 K, it took about 2 min to anodize a 1 μm aluminum layer completely. The anodization process was stopped at the moment that strong gas evolution occurred

(26) Lebedeva, V. N.; Distler, G. I.; Grechusnikov, Y. N. *Sov. Phys.-Dokl.* **1966**, *11*, 241.
(27) van der Zande, B. M. I.; Pagès, L.; Hikmet, R. A. M.; van Blaaderen, A., submitted to *J. Phys. Chem. B.*
(28) Diggle, J. W.; Downie, T. C.; Goulding, C. W. *Chem. Rev.* **1969**, *69*, 365.
(29) Keller, F.; Hunter, M. S.; Robinson, D. L. *J. Electrochem. Soc.* **1953**, *100*, 411.

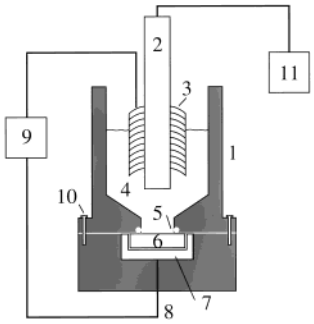

Figure 2. Anodization setup. The numbers represent (1) Teflon cell, (2) rotating disk, (3) platinum counter electrode, (4) electrolyte solution (15 v/v% H_2SO_4), (5) O-ring, (6) the substrate of Figure 1 serving as the working electrode (WE), (7) the conductive sample holder, (8) WE contact, (9) the power supply, (10) screws, and (11) rotating disk motor.

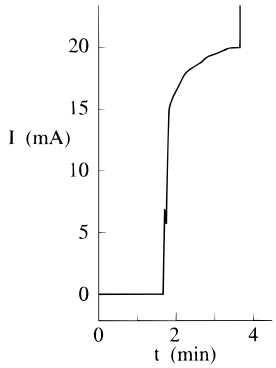

Figure 3. Anodization current (I) as a function of time (t) during the anodization process of alumina. The steady-state current is 20 mA/membrane area, which is 35 mA/cm^2.

because of reduction of water at the platinum cathode accompanied with an increase in current up to 2 A·cm^{-2}. The initial pore diameter, which equals 12 nm, can be increased by slow dissolution of alumina in a 1 v/v % H_3PO_4 solution,[8,10] which resulted in a pore diameter of 22 nm. We found that for our system the dissolution rate of the alumina was 0.8 nm·min^{-1}.

After the anodization process, the porous alumina has a thickness of 1.5 μm, a pore density of about 8×10^{14} m^{-2}, and an average pore diameter of 12 ± 3 nm as determined by field emission gun scanning electron microscopy (FEG-SEM) and transmission electron microscopy (TEM). The average spacing between the pores is about 30 nm. Figure 4 shows a typical FEG-SEM micrograph of the obtained porous alumina. The cross section (Figure 4b) shows that the pores are oriented parallel to each other. The top view (Figure 4a) shows the random distribution of the pores. The apparent domain structure present on the FEG-SEM picture is most likely caused by the grain structure of the initial aluminum layer. The pore formation seems to be favored at the grain boundaries.

No hexagonal structure is present in contrast to the models of anodization[28−32] and experimental results.[33] This is mainly caused by the fast anodization process (i.e., 2 min compared to 160 h[33]) and the high temperature (i.e., room temperature compared to 0 °C[33]).

Gold Sol Synthesis. The electrodeposition was performed in the same Teflon cell as was used during the anodization process. The substrate did not have to be removed from the holder, which is very convenient for practical reasons such as the wetting of the pores and the positioning of the substrate. Three electrodes were used during the electrodeposition stages instead of a two-electrode system as in the anodization process. Figure 5 shows the setup of the electrodeposition. A saturated calomel electrode (SCE) served as the reference electrode (2) and was placed at a distance of about 6 mm above the working electrode (6) (the substrate). The counter electrode (3) was the same platinum electrode as was used during anodization. The constant voltage was applied by a PAR 273A (EG&G Princeton Applied Research) potentiostat/galvanostat.

Prior to electrodeposition of gold, a small amount of copper was needed.[10,13] Copper can be selectively dissolved, which enables the release of the gold rods from the support. The copper deposition took place for 100 s at a constant voltage of −0.05 V vs SCE using an aqueous 0.01 M copper-(II) sulfate solution with a pH between 1 and 2 (0.1 M sulfuric acid); see Figure 6, stage I. Between stages I and II (electrodeposition of gold) an extra electrodeposition step was applied to deposit copper ions, which may still be present in the nanopores after removal of the copper electrolyte. This electrodeposition step was performed in a 0.01 M H_2SO_4 solution (without copper) with a constant voltage of −0.2 V vs SCE. It turned out that this extra

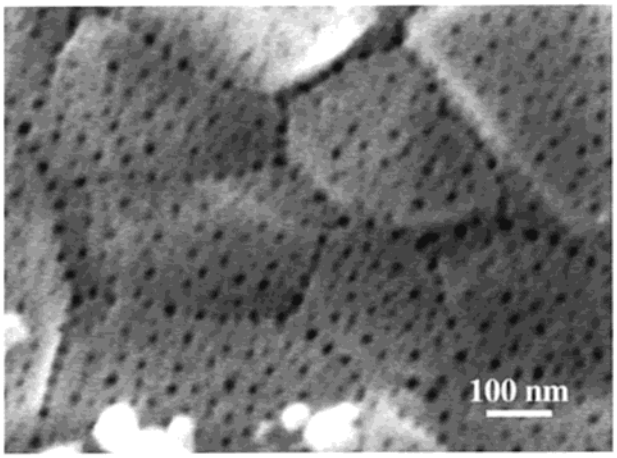

a)

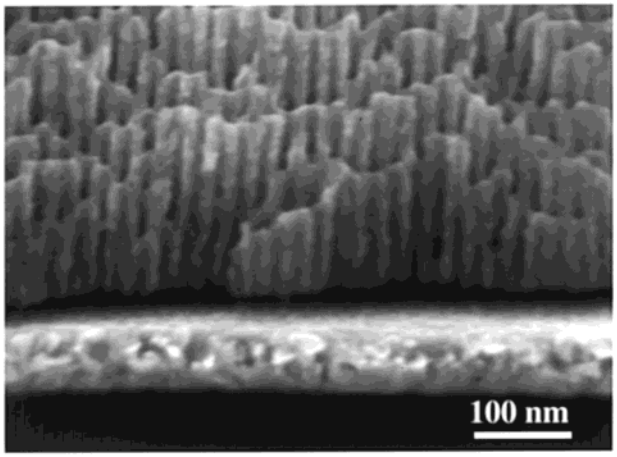

b)

Figure 4. FEG-SEM picture of the alumina membrane: (a, topview) orientation of the pores; (b, cross section) parallel orientation of the pores. The pore diameter is 12 nm.

(30) Heber, K. V. *Electrochim. Acta* **1978**, *23*, 127.
(31) Heber, K. V. *Electrochim. Acta* **1978**, *23*, 135.
(32) Despic, A.; Parkhutik, V. P. In *Modern aspects of electrochemistry*; Bockris, J. O. M., White, R. E., Conway, B. E., Eds.; Plenum Press: New York, 1989; Part 2, Chapter 6.
(33) Masuda, H.; Fukuda, K. *Science* **1995**, *268*, 1466.

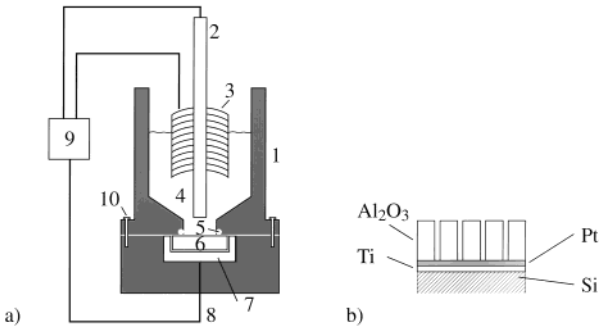

Figure 5. (a) Schematic representation of the electrochemical cell. Instead of a two-electrode system as was used for the anodization, a three-electrode setup is used. The numbers represent (1) Teflon cell, (2) standard calomel electrode, (3) platinum counter electrode, (4) electrolyte solution (gold(I) cyanide), (5) O-ring, (6) alumina membrane serving as the working electrode (WE), (7) conductive sample holder, (8) WE contact, (9) potentiostat, and (10) screws. (b) Working electrode consisting of a silicon substrate covered with successively a thin layer of titanium (10 nm) and a platinum electrode (75 nm) and the porous alumina (1.5 Tm).

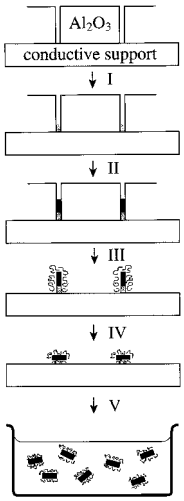

Figure 6. Schematic representation of the successive stages to obtain aqueous dispersions of gold rods starting from the alumina membrane. The first stage (I) involves the electrodeposition of copper followed by the electrodeposition of gold (II). Subsequently, the membrane (III) and the copper (IV) are selectively dissolved to release the rods. By ultrasonication the rods are dispersed in water (V).

electrodeposition step narrowed the length distribution. Subsequently, gold was deposited on top of the copper (Figure 6, stage II). An aqueous 0.32 M gold(I) cyanide solution containing 0.26 M citric acid and 0.65 M KOH with a final pH between 5 and 6 was used for the electrodeposition of gold in the nanopores of alumina. The typical current density was about 70 mA·cm^{-2} membrane area. Because the total pore area (actual deposition area) was estimated to be only 10% of this area, the actual current density in the pores was a factor of 10 higher.

Stage III involves the dissolution of the aluminum oxide in an aqueous 1.25 M NaOH solution[13] in the presence of 4 g·L^{-1} PVP for 5−10 min, followed by dissolution of the copper using a 1:100 diluted copper etchant in an aqueous solution of 4 g·L^{-1} PVP. The composition of the aqueous copper etchant was 25 mL·L^{-1} 98% H_2SO_4, 175 mL·L^{-1} 30% H_2O_2, and a few drops of 85% H_3PO_4. The detached rods were lying on the substrate after 30 min of exposure to the copper etchant. The samples were rinsed with demineralized water after each stage. Finally, the rods grown in several membranes were combined to increase the number concentration of rods required to perform measurements. About 5−10 samples were used to obtain 1 mL of dispersion. The particles were dispersed in demineralized water by ultrasonication (SONIPREP 150, Sanyo). The power used for ultrasonication has to be moderate to prevent flocculation and breaking of the silicon wafer. Another dispersion medium other than water can, in principle, be chosen at this stage of dispersion preparation in contrast to other preparation methods because the rods stay on the surface after dissolution of the copper.

To be able to disperse the rods, a suitable stabilizer had to be chosen, which is facilitated by the extensive documentation on gold sol stabilization.[34−37] Addition of citrate[35] does not result in a stable dispersion. Large flocs are observed immediately after release from the substrate. Citrate adsorption does not lead to stabilization because the double-layer repulsion is too weak because of the high ionic strength of the etchants and the (temporary) presence of copper and aluminum ions. However, it is known from the literature on the stabilization of noble metals[34,36,38−40] that steric stabilization can be achieved by using uncharged polymers with elements having a free electron pair such as N, S, O, and P. We found that addition of 4 g·L^{-1} PVP to the sodium hydroxide solution and copper etchant results in a stable dispersion. No aggregation or gelation is visually observed.

The colloidal stability of the dispersions synthesized is investigated in more detail with dynamic light scattering and electrophoresis both described in ref 41. It is demonstrated that indeed single particles are present in solution.

The absorbance behavior of aqueous dispersions of gold rods was studied with visible near-infrared (vis/NIR) spectroscopy (Perkin-Elmer UV/vis/NIR Lambda 9 double-beam spectrophotometer) using a cuvette with optical path length $x = 1$ cm.

Theory

Absorbance of Light by Metallic Colloidal Particles. In the following we mainly follow the notation in ref 42. The absorbance (or extinction), A, of the incident light includes both scattering and absorption contributions and is defined as

$$A = -\ln \frac{I}{I_0} = \gamma x \qquad (1)$$

where I_0 is the intensity of the incident light beam, I is the intensity after the beam has traversed a distance x through the medium, and γ is the extinction coefficient.

Spheres. As a starting point, we will use the equations for the extinction coefficient in the dipole approximation. In the dipole approximation the expression for the extinction coefficient becomes

(34) Roescher, G. A. Stabilization of colloidal noble metals by block copolymers. Thesis, University Twente, Twente, The Netherlands, 1995.
(35) Frens, G. *Nature* (*London*), *Phys. Sci.* **1973**, *241*, 20.
(36) Thiele, H.; Kowallik, J.; *Kolloid Z. Z. Polym*. **1969**, *234*, 1017.
(37) Handley, D. A. In *Colloidal gold, principles, methods, and applications*; Hayat, M. A., Ed.; Academic Press Inc.: New York, 1989; Chapter 2.
(38) Hirai, H. *J. Macromol. Sci. Chem. A13* **1979**, *5*, 633.
(39) Hoogsteen, W.; Fokkink, L. G. J. *J. Colloid Interface Sci*. **1995**, *175*, 12.
(40) Huang, H. H.; Ni, X. P.; Loy, G. L.; Chew, C. H.; Tan, K. L.; Loh, F. C.; Deng, J. F.; Xu, G. Q. *Langmuir* **1996**, *12*, 909.
(41) van der Zande, B. M. I.; Dhont, J. K. G.; Böhmer, M. R.; Philipse, A. P., submitted to *Langmuir*.
(42) Papavassiliou, G. C. *Prog. Solid State Chem*. **1979**, *12*, 185.

$$\frac{\gamma}{N_p V} = \frac{18\pi\epsilon_\alpha^{3/2}}{\lambda} \frac{\epsilon_2}{(\epsilon_1 + 2\epsilon_\alpha)^2 + \epsilon_2^2} \quad (2)$$

where N_p represents the number concentration of particles, V the single particle volume, λ the wavelength of light in a vacuum, and M_I the dielectric constant of the surrounding medium and ϵ_1 and ϵ_2 are the real ($n^2 - k^2$) and imaginary ($2nk$) parts of the complex refractive index of the particles. In this equation it is assumed that the medium does not absorb the incident light. The dielectric constant of the medium, ϵ_α, can then be expressed as

$$\epsilon_\alpha = n^2 \quad (3)$$

The origin of the color of a dispersion containing metal particles lies in the denominator of eq 2, which predicts the existence of an absorbance peak when

$$\epsilon_1 + 2\epsilon_\alpha = 0 \quad (4)$$

A strong aborbance peak is present if M_2 is relatively small compared to M_1, which certainly holds for gold.[43] The real part of the complex refractive index changes from almost zero to −200 when the wavelength changes from 300 to 2200 nm, whereas the imaginary part of the complex refractive index is between 0 and 5 in this wavelength regime.

Randomly Oriented Elongated Ellipsoids. To account for the anisotropy and, consequently, for the orientation dependence of the plasmon oscillation, Gans[19] introduced a geometrical factor P_j to calculate the absorbance of light by ellipsoids. The geometrical factor corresponds to each of the axes A, B, and C of the particle as indicated in Figure 1. Gans' formula for randomly oriented elongated ellipsoids in the dipole approximation is[42]

$$\frac{\gamma}{N_p V} = \frac{2\pi\epsilon_\alpha^{3/2}}{3\lambda} \sum_{j=A}^{C} \frac{\left(\frac{1}{P_j^2}\right)\epsilon_2}{\left[\epsilon_1 + \left(\frac{1 - P_j}{P_j}\right)\epsilon_\alpha\right]^2 + \epsilon_2^2} \quad (5)$$

For elongated ellipsoids (or rods) the B and C axes are equal and correspond to the particle diameter (d) while the A axis represents the particle length (L). The geometrical factors P_j for elongated ellipsoids along the A and B/C axes are respectively given by[42]

$$P_A = \frac{1 - e^2}{e^2}\left[\frac{1}{2e}\ln\left(\frac{1 + e}{1 - e}\right) - 1\right] \quad (6)$$

$$P_B = P_C = (1 - P_A)/2 \quad (7)$$

with

$$e = \left(\frac{L^2 - d^2}{L^2}\right)^{1/2} \quad (8)$$

The total absorbance of randomly oriented elongated ellipsoids is the summation over the three dimensions in which plasmon oscillation can occur. In analogy with the absorbance of spheres, the wavelength at which the plasmon resonates is given by

$$\epsilon_1 + \left(\frac{1 - P_j}{P_j}\right)\epsilon_\alpha = 0 \quad (9)$$

Here, $(1 - P_j)/P_j$ is called the screening parameter R_j which strongly depends on the anisotropy of the particle as shown in Figure 7. For rods with a given aspect ratio, two values of the screening parameter exist: $R_B = R_C$ corresponds to the transverse plasmon oscillation, and R_A represents the longitudinal oscillation. With increasing aspect ratio, the screening parameter of the longitudinal oscillation shifts toward infinity, while in the case of the transverse oscillation, the screening parameter reaches 1.

Calculated Spectra for Colloidal Gold Rods. Figure 8 shows the absorbance spectra calculated with eq 5 using the bulk optical parameters for gold from ref 39 and the refractive index of water (1.333). The dependence of λ_{max} on the aspect ratio is most pronounced in the longitudinal resonance, which has been confirmed experimentally.[44] The maximum of the longitudinal absorbance band ($\lambda^{\parallel}_{max}$) shifts to longer wavelengths with increasing aspect ratio. Less pronounced, but also an effect of the aspect ratio, is the small shift of the transverse resonance maximum ($\lambda^{\perp}_{max}$) to shorter wavelengths with increasing aspect ratio.[7,21−23] Both shifts can be attributed to the change in the screening parameter. Two other consequences of increasing anisotropy are present. First, damping of the transverse resonance occurs (Figure 8b). This is attributed to the change in P_B and P_C (i.e., shape of the particle), and the sharp decrease of M_2 in the wavelength region of 450−550 nm. Second, the maximum extinction of the longitudinal plasmon band increases with anisotropy, which is caused by the decrease in P_A.

Results and Discussion

Figure 9 shows TEM pictures of the gold rods with aspect ratios ranging from L/d = 1.8 to 49. Apart from the cylindrical rods, some of the rods have side branches or surface irregularities, which are both attributed to the pore geometry. The size distribution in rod length (σ_L/L) varies from 10 to 25%. In general, 30−100 rods were measured for each dispersion. The number-averaged lengths and diameters as well as their standard deviations are presented in Table 2. The systems are coded as, e.g., ROD12.6, in which the number refers to the aspect ratio. The relative polydispersity in length tends to decrease with increasing rod length. The absolute polydispersity in diameter (σ_d) is almost constant. The gold concentration in the dispersions is 10^{-5}−10^{-4} g·mL^{-1}. X-ray diffraction showed that the growth of the rods in pores led to polycrystalline gold with a preferential (100) orientation, whereas a continuous film of electrodeposited gold under the same conditions had a preferential orientation of (111).

Figure 10 shows the particle length L, determined by analysis of the TEM micrographs, plotted against the deposition time. The particle length increases with deposition time. However, at a given deposition time dispersions with various lengths are obtained (e.g., t_{dep} = 135 s, indicated with the arrow in Figure 10). It is found that a temperature difference of approximately 3.5 °C leads to a difference in length of approximately 20 nm. For practical reasons we did not use a thermostated electrodeposition cell. The procedure of mixing several samples may account for the observed polydispersity. Furthermore, indications are obtained that the use of old gold cyanide

(43) *Optical properties of metals*; Weaver, J. H., Krafka, C., Lynch, D. W., Eds.; Physics Data Series No. 18-2; Fachinformationzentrum: Karlsruhe, Germany, 1981; Vol. 2.

(44) Lisiecke, I.; Billoudet, F.; Pileni, M. P. *J. Phys. Chem.* **1996**, *100*, 4160.

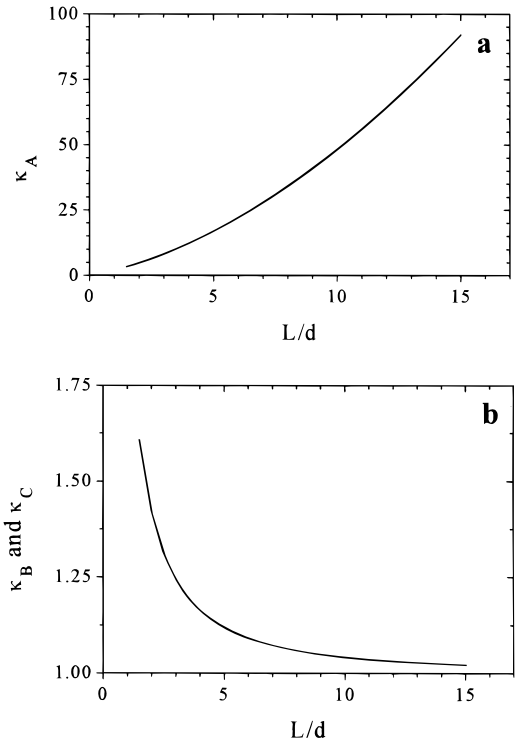

Figure 7. Screening parameter R_j along the *A* axis (a) and along the *B* and *C* axes (b) plotted against the aspect ratio (*L*/*d*).

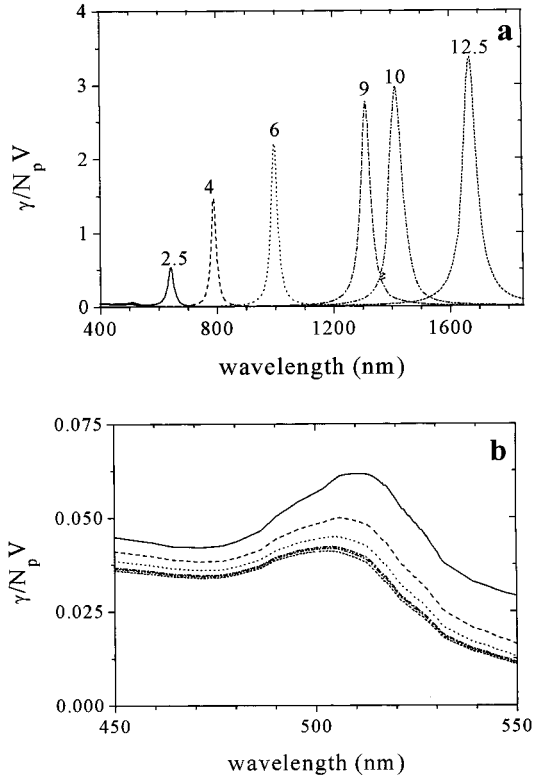

Figure 8. Absorbance spectra calculated with the expressions of Gans for elongated ellipsoids (eq 5) using the bulk optical data for gold.[39] In part b only the wavelength regime 450−550 nm is plotted to show the transverse resonance. The line format is identical with that in part a. The numbers on the spectral curves indicate the aspect ratio (*L*/*d*).

solutions and inhomogeneous nucleation of the electrodeposition of gold may contribute to the polydispersity.

A remarkable characteristic of the gold rod dispersions is the aspect ratio dependent color. The dispersion of rod-shaped particles with $L/d = 2.6$ was of a blue-grayish color, while a dispersion of rods with an aspect ratio exceeding 4 was red-brownish. The brownish color is caused by the enhanced scattering due to the increased particle size.[45] The absorbance spectra are shown in Figure 11. The spectra show that the optical properties of the dispersion change markedly with the aspect ratio, which is in analogy with the results obtained in refs 21 and 24. To clarify the shift of the resonances with increasing aspect ratio, both the longitudinal and transverse maxima (λ_{max}) are plotted against the aspect ratio in Figure 12. Qualitative agreement is obtained with the predicted longitudinal peak positions within the experimental error. Quantitatively, however, the experimental λ_{max} values slightly deviate from those calculated: resonance occurs at longer wavelengths compared to the calculated peak positions. Furthermore, the width of the experimental resonance bands is considerably larger than those calculated.

Both aspects may be caused by multipole contributions (which are not taken into account in the used expressions). Because Mie has shown that the absorbance maximum of spheres is shifted to longer wavelengths because of multipole contributions and scattering, the peak is broadened and the maximum is decreased.[46,47] The extent of a peak shift due to the multipole contributions is considerable. For instance, for gold spheres with diameters of 10 (no multipole contributions), 60, and 120 nm embedded in alumina, the absorbance maximum occurs at wavelengths of 545, 556, and 658 nm, respectively.[7]

To verify whether multipole contributions affect the peak positions of the longitudinal resonance, we synthesized particles with the same aspect ratio (*L*/*d*) but different sizes (e.g., dispersions 2 (53/12.5) and 4 (82/19) or dispersions 7 (99/11) and 12 (152/17)). No effect of size on the longitudinal peak position is measured within the experimental error for the dispersion numbers 2, 4, and 6 as well as the dispersion numbers 7, 10, and 12. This shows that the multipole contributions do not significantly affect the absorbance peak position in the studied size regime although the particle dimensions are on the order of the resonance wavelength of light. Apparently, the Gans theory for elongated ellipsoids in the dipole approximation can be used to predict the longitudinal resonance positions. The effect of size on ($\lambda^{||}_{max}$) is probably absent for the studied particle dimensions, because the particle diameter is much smaller than the resonance wavelength.

The discrepancy between experiment and theory is attributed to the polydispersity in shape ($\sigma_{L/d}$ as listed in Table 2). The origin of the peak shift induced by polydispersity results from the larger particles which contribute more to the absorbance of light than the smaller particles, as demonstrated in Figure 8. The maximum absorbance increases with increasing aspect ratio, especially in the *L*/*d* regime $2 < L/d < 6$. The maximum absorbance is extremely sensitive to the shape in this regime. Consequently, λ_{max} is shifted to longer wavelengths as compared to the λ_{max} predicted by eq 5 using the number-averaged TEM data for the shape. The experimental data indeed show that the peak positions obtained for the dispersions with the smallest relative polydispersity in shape (as listed in Table 2) approach the predicted values most closely. The open symbols in Figure 12a indicate the

(45) Bohren, C. F.; Huffman, D. R. *Absorption and scattering of light by small particles*; Wiley: New York, 1983.
(46) Wilcoxon, J. P.; Williamson, R. L.; Baughman, R. *J. Chem. Phys.* **1993**, *98*, 9933.
(47) Turkevich, J.; Garton, G.; Stevenson, P. C. *J. Colloid Sci.* (*Suppl. 1*) **1954**, *26*.

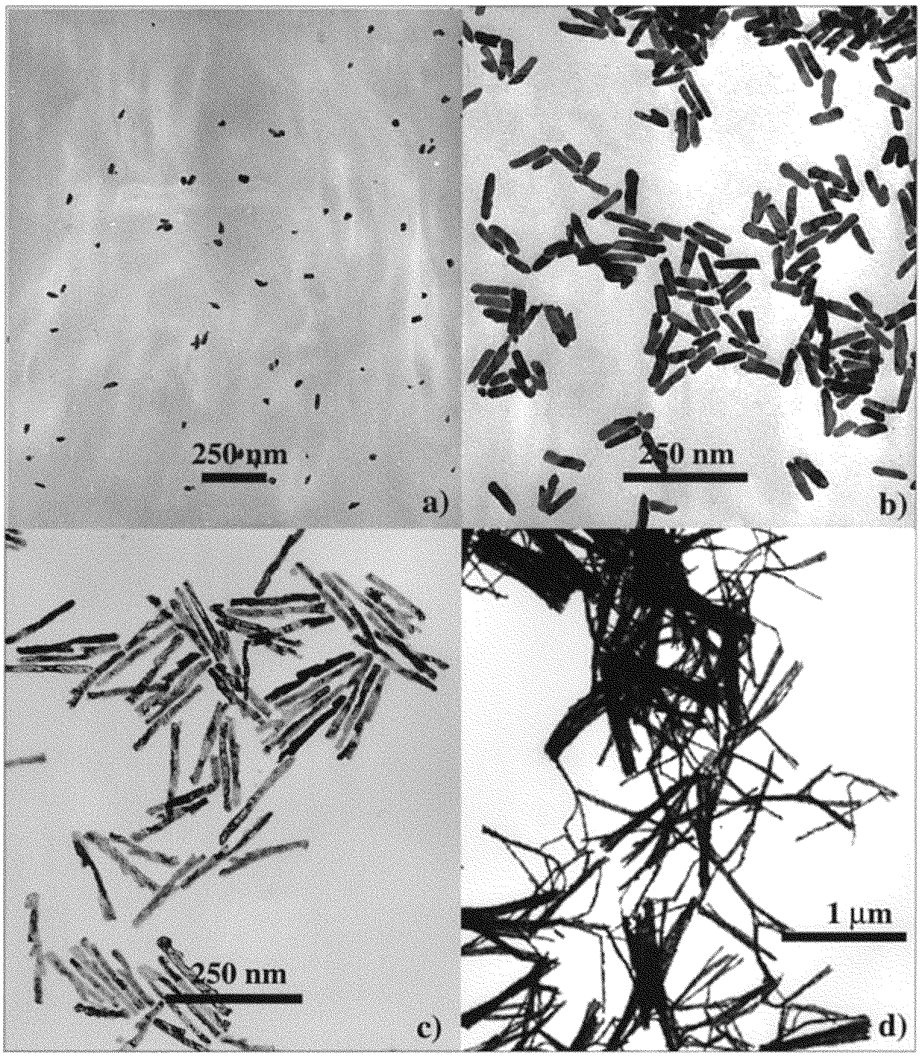

Figure 9. TEM micrographs of gold rods: (a) $L = 40$ nm, $d = 22$ nm; (b) $L = 82$ nm, $d = 19$ nm; (c) $L = 189$ nm, $d = 15$ nm; (d) $L = 729$ nm, $d = 15$ nm.

Table 2. Particle Dimensions of the Template Synthesized Gold Rods and the Positions of the Transverse ($\lambda^{\perp}_{max}$) and Longitudinal ($\lambda^{||}_{max}$) Absorbance Maxima[a]

no.	L (nm)	σ_L (nm)	d (nm)	σ_d (nm)	L/d	$\sigma_{L/d}$	$\lambda^{\perp}_{max}$ (nm)	$\lambda^{||}_{max}$ (nm)
1	40	9	22	4	1.8	0.8	539	646
2	53	17	12.5	3	4.2	2.4	524	870
3	47	20	18	4	2.6	1.7	525	746
4	82	9	19	3	4.4	1.3	518	860
5	106	12	20	3	5.3	1.3	516	950
6	63	30	16	3	3.9	2.6	525	908
7	99	23	11	3	9	4.5	519	1224
8	103	33	15	2	6.9	3.1	513	1220
9	92	15	16	2	6.1	1.7	514	1054
10	146	37	16.6	3	8.9	3.9	515	1290
11	165	31	12.5	3	13.2	5.7	518	
12	152	30	17	2	8.9	2.9	513	1240
13	190	27	19	3	10	3.0	519	1398
14	249	30	20	3	12.5	3.4	519	1732
15	283	22	20	3	14.2	3.3	517	
16	259	54	15	2	17.2	6.4	512	

[a] The particle dimensions are determined by analysis of the transmission electron micrographs. L = number-averaged particle length. d = number-averaged diameter. σ_x = standard deviation of x.

results of the dispersions with the smallest relative polydispersity $\sigma_{L/d} \approx 25\%$.

In addition, polydispersity induces peak broadening.

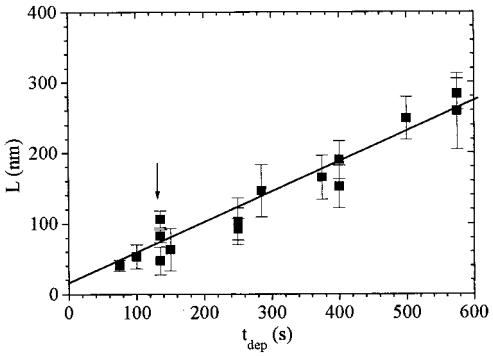

Figure 10. Length (L) of the gold rods deduced from the TEM micrographs as a function of the deposition time (t_{dep}). The solid line represents a linear fit through the data points. The arrow indicates an example of three dispersions with different lengths but prepared with the same deposition time.

Therefore, the width of the bands presented in Figure 11 is much broader than that theoretically predicted in Figure 8. We have fitted the absorbance band with a Gaussian. It is found that the standard deviation obtained from the fit corresponds to that in L/d as determined by TEM given in Table 3. This indicates that the peak broadening can be ascribed to the polydispersity in shape. A similar conclusion was reached by Chang et al.,[4] who studied rods of very similar dimensions.

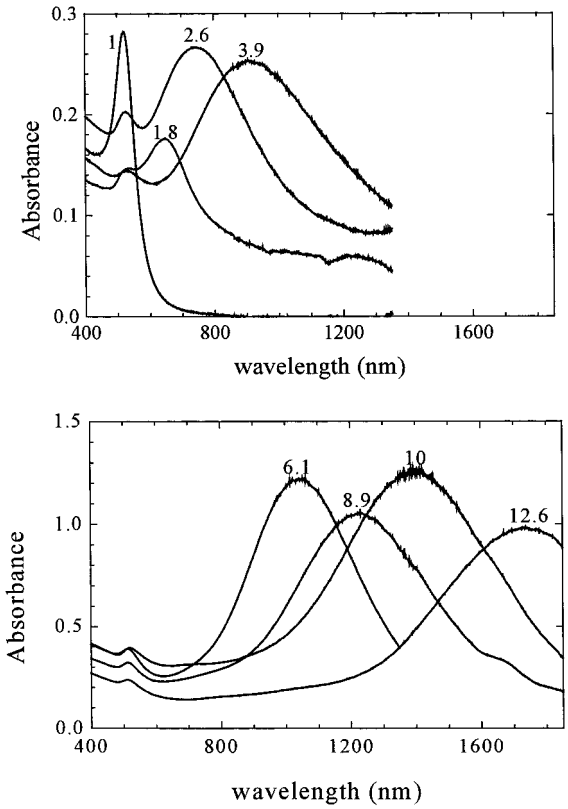

Figure 11. Experimental vis/NIR absorbance spectra of rod dispersions with varying aspect ratios (denoted by the numbers on the spectral curves) and one of a sphere dispersion (indicated by 1). For a few dispersions the gold rods are dispersed in deuterium oxide. Consequently, the absorbance can be monitored in the wavelength range 400−1800 nm instead of 400−1350 nm, which was the experimental regime of water in this study.

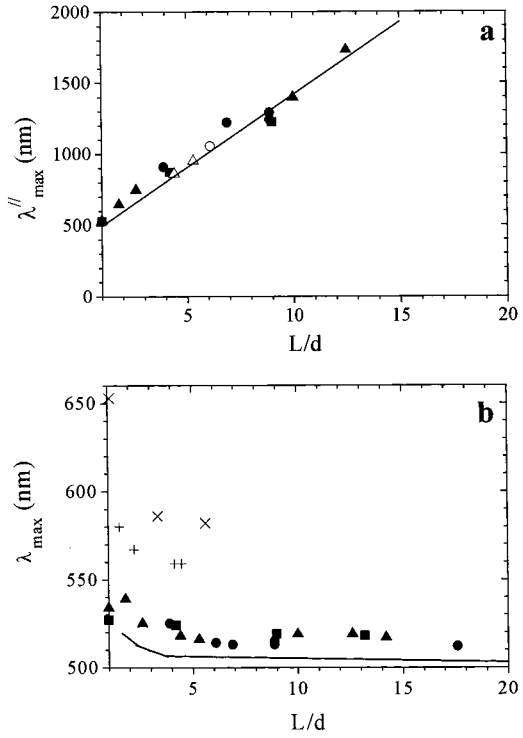

Figure 12. Positions of the plasmon absorption maxima of the longitudinal, $\lambda^{\parallel}_{max}$ (a), and the transverse, $\lambda^{\perp}_{max}$ (b), resonance plotted against the aspect ratio (L/d). The experimental data obtained in this study for rods with $d = 12$ (■), 16 (●), and 20 nm (▲), the data calculated with eq 5 (solid line), and the results taken from ref 7 (+ represents $d = 86$ nm and × $d = 120$ nm) are included. The open symbols indicate the dispersions with narrow size distributions. Note that in ref 7 the gold rods are embedded in alumina instead of water.

Figure 12b includes the transverse resonance results from ref 6 for gold rods with $d = 86$ and 120 nm embedded in alumina. Note that alumina has a refractive index equal to 1.6,[7] whereas that of water equals 1.333. The change in refractive index leads to a peak shift of about 20 nm to longer wavelengths in the case of gold spheres with a diameter of about 15 nm. Nevertheless, these results show that the diameter influences the position of the absorbance maxima. Our results for the transverse resonance for rods with a diameter in the range of 12 nm < d < 22 nm are between the experimental results of Foss et al.,[7] who studied systematically the influence of the diameter on the transverse resonance and the calculations for rods in the limit of infinitely small particles (eq 5). Therefore, we conclude that our transverse resonance results are consistent with the results obtained with eq 5 and the results presented in ref 7. A significant effect of the diameter on the transverse resonance can only be measured for extremely monodisperse systems for rods with radii in the range we prepared in this study.

Conclusions

Nearly monodisperse gold rods with adjustable aspect ratios are made by electrodeposition of gold in nanopores of alumina. The gold rods are dispersed in an aqueous medium by dissolution of the membrane and detachment from the substrate. Coagulation of the particles is prevented by steric repulsion caused by PVP adsorption.

The optical properties of aqueous dispersions of colloidal gold rods depend strongly on the aspect ratio of the particles. Because of the anisotropy, the absorbance spectra of randomly oriented colloidal gold rods display a longitudinal and a transverse resonance contribution. With increasing anisotropy, the maximum of the longitudinal resonance is shifted to the infrared and the maximum of the transverse resonance is shifted to smaller wavelengths. The experimental data for the longitudinal resonance agree with the Gans theory for elongated ellipsoids in the dipole approximation. It has been shown that the multipole contributions are virtually absent in the longitudinal resonance. The small shift of the transverse resonance to shorter wavelengths is consistent with the results presented in the literature and the Gans theory.

Acknowledgment. The authors thank the people in the analysis department (Centre For manufacturing Technology (CFT), Eindhoven, The Netherlands) for the chemical and structure analysis (TEM and SEM). Dr. M. P. C. Krijn (PRL) is acknowledged for making the FEG-SEM images. Dr. A. v. Petukhov (Research Institute for Materials, University Nijmegen) is aknowledged for carefully reading the manuscript. Prof. Dr. H.N.W. Lekkerkerker and Prof. Dr. A.P. Philipse (Van't Hoff Laboratory for Physical and Colloid Chemistry, Utrecht University, Utrecht, The Netherlands) are acknowledged for stimulating discussions. This work is part of the research program of the Foundation for Fundamental Research on Matter (FOM) with financial support from The Netherlands Organization for Scientific Research (NWO).

LA9900425